processes

MDPI

Article

Preparation of Bioaerogel from Iron-Rich Microalgae for the Removal of Water Pollutants

Xinqi Niu [1,2,3], Junhui Si [1,2,3], Binyi Chen [1,2,3], Qianting Wang [1,2,3,*], Sen Zeng [1,2,3,*] and Zhixiang Cui [1,2,3,*]

[1] College of Materials Science and Engineering, Fujian University of Technology, Fuzhou 350118, China; m15225469596@163.com (X.N.)
[2] Fu Jian Provincial Key Laboratory of Advanced Materials Processing and Application, Fuzhou 350118, China
[3] Key Laboratory of Polymer Materials and Products of Universities in Fujian, Fujian University of Technology, Fuzhou 350118, China
* Correspondence: cocolark@163.com (Q.W.); zengs@fjut.edu.cn (S.Z.); cuizhixiang2006@126.com (Z.C.)

Abstract: Microalgae-based materials have gained significant attention considering their rich resources, cost-effectiveness, and environmental friendliness. Herein, iron-rich microalgae (Chlorella pyrenoidosa, CP) were treated by hydrothermal reaction under alkaline conditions to remove the protoplast and obtain a hollow shell with an Fe_xO_y core inside. Then, the iron-rich microalgae-based aerogel (Fe-CP aerogel) was fabricated through a freeze-drying process. The as-prepared Fe-CP aerogel exhibited superior adsorption performance, and the maximum adsorption quantity for Cu^{2+} could reach 208.3 mg/g due to the synergistic adsorption of the hollow shell of CP cells and Fe_xO_y core. The Fe-CP aerogel also possessed super-hydrophilicity and displayed high separation efficiency (over 99%) when used for separating different oil/water emulsions. Moreover, the existence of Fe_xO_y endowed the Fe-CP aerogel with photo-Fenton activity, thus exhibiting excellent antifouling performance. The prepared Fe-CP aerogel could be considered an ideal adsorbent, with green, efficient, low-cost, and regenerative properties, and has the potential for the practical treatment of wastewater.

Keywords: microalgae; aerogel; adsorption; wastewater treatment; photo-Fenton

check for updates

Citation: Niu, X.; Si, J.; Chen, B.; Wang, Q.; Zeng, S.; Cui, Z. Preparation of Bioaerogel from Iron-Rich Microalgae for the Removal of Water Pollutants. *Processes* **2024**, *12*, 1313. https://doi.org/10.3390/pr12071313

Academic Editor: Andrea Petrella

Received: 15 May 2024
Revised: 19 June 2024
Accepted: 20 June 2024
Published: 24 June 2024

Copyright: © 2024 by the authors. Licensee MDPI, Basel, Switzerland. This article is an open access article distributed under the terms and conditions of the Creative Commons Attribution (CC BY) license (https://creativecommons.org/licenses/by/4.0/).

1. Introduction

Water pollution including heavy metal ions, organic dyes, and oily wastewater possessing negative impacts on living organisms has been one of the major concerns and challenges to the environment and economy [1,2]. The accumulation of these complex contaminants in the natural environment will be mutagenic, teratogenic, and carcinogenic to humans; however, eliminating these microcontaminants is difficult [3–5]. Hence, the development of efficient and green approaches to remove the contaminants in water is urgent and significant.

Several methods, such as catalytic degradation, adsorption, chemical precipitation, bio-degradation, and membrane separation, have been proposed [6–8]. Adsorption is considered as a promising method to remove metal ions, organic dyes, and oily wastewater considering its simple operation, high efficiency, and sustainable properties [9]. Until now, many porous materials (e.g., activated carbons, carbon nanotubes, metal oxide, graphene, and metalorganic frameworks) have been extensively explored [10]. Although many of them possessed excellent adsorption capability, most of them exhibited the ubiquitous shortcomings of high cost, non-degradability, complex preparation, and possible secondary pollution [11]. Hence, it is essential to develop adsorbents that possess large adsorption capacity and overcome these drawbacks simultaneously. Moreover, the selectivity against other ions, long-term stability, cyclic regeneration, and antifouling properties of the adsorbent are also very important [12]. Hence, it is essential to develop novel adsorbents that can meet these requirements.

Natural biological adsorbent materials with several merits, such as low cost, abundant resources, degradability, and green qualities, have been regarded as ideal candidates for contaminant removal [12,13]. He et al. reported a carboxylated wood aerogel prepared by delignification and the in situ oxidation treatment of natural balsa wood that exhibited an adsorption quantity of 115 mg/g for Cu^{2+} [14]. Cellulose nanofiber (CNF)/gelatin aerogel was prepared to remove dyes by adsorption, and the maximum adsorption quantities for Congo red and methylene blue were 590.6 and 182.6 mg/g, respectively [15].

Recently, microalgae have notably received considerable attention [16,17]. The abundant microalgae resources provide a large amount of raw materials for the large-scale preparation of microalgae-based adsorbents [18–20]. In particular, harmful microalgae can grow very fast, forming a large amount of phytoplankton and water blooms and leading to the eutrophication of water quality [21]. Therefore, the utilization of microalgae to prepare biological adsorbents that change waste into valuables is of great significance. Microalgae-based materials possess numerous active groups, such as amino, hydroxyl, and carboxyl, which can advance the efficiency of adsorption [22,23]. However, on the one hand, a critical issue of using microalgae is that they are difficult to collect after the adsorption process in solutions [24]. On the other hand, adsorbents are commonly limited by their low regeneration efficiency and thus hard to recycle, especially for organic pollutants [25]. To address these issues, microalgae were prepared in bulk materials or loaded on porous material. For example, Singhal et al. [26] prepared an aerogel constructed by microalgae and chitosan, which exhibited an adsorption quantity of 300 mg/g and 250 mg/g in freshwater and seawater. However, these aerogel adsorbents will be seriously affected by the fouling caused by organic pollutants and microorganisms [27]. Consequently, the development of novel microalgae-based adsorbents combined with high adsorption capacity and antifouling ability is crucial to realizing practical applications.

Aerogels have attracted extensive attention and are explored as novel adsorbent materials due to the unique advantages of high porosity, ultra-low density, and excellent adsorption ability [28]. Herein, an all-natural microalgae-based aerogel was developed as an adsorbent and used for the removal of contaminants from water. The morphology, composition, and structure of the aerogel were characterized. The adsorption and separation performances of the aerogel for different pollutants were evaluated. The designed aerogel is purely based on algae with excellent adsorption ability and antifouling performance and showed great potential application in wastewater treatment.

2. Experimental Section

2.1. Materials

The *Chlorella pyrenoidosa* (CP) was supplied by the Wuhan Hydrobiology Institute of the Chinese Academy of Sciences. BG-11 culture medium was obtained from Shanghai Guangyu Biotechnology Co., Ltd. (Shanghai, China) Ligroin, n-hexane, kerosene, hydrochloric acid (HCl), rhodamine b (RB), and methylene blue (MB) were supplied by Xilong Chemical Reagent Co., Ltd. (Guangzhou, China) Copper sulfate ($CuSO_4$) and sodium dodecyl sulfate (SDS) were provided by Tianjin Zhiyuan Chemical Reagent Co., Ltd. (Tianjin, China).

2.2. Preparation of the Fe-CP Aerogels

CP was cultured in BG-11 medium under illumination in an incubator with a temperature of 25 °C. After a period of cultivation, CP was collected using the coagulation method, and the $FeCl_3$ (100 mg/L) was added and kept for 15 min. Then, the iron-rich CP (Fe-CP) biomass was harvested with centrifugation and dried in an oven at 65 °C. The obtained biomass (10 g) was mixed with alkaline solution (80 mL, pH = 12), and then the SDS solution (2% *w*/*v*, 80 mL) was added. The mixture was kept in an oven at 90 °C for 3 h. The treated Fe-CP biomass was recovered and washed with DI water three times. Subsequently, 0.5 g of the obtained biomass was added to the deionized water (50 mL) and heated and kept at 160 °C for 2 h. The obtained biomass was recovered by centrifugation

and washed three times, and then added into a customized mold and freeze-dried by freeze-dryer for 12 h, as illustrated in Figure 1.

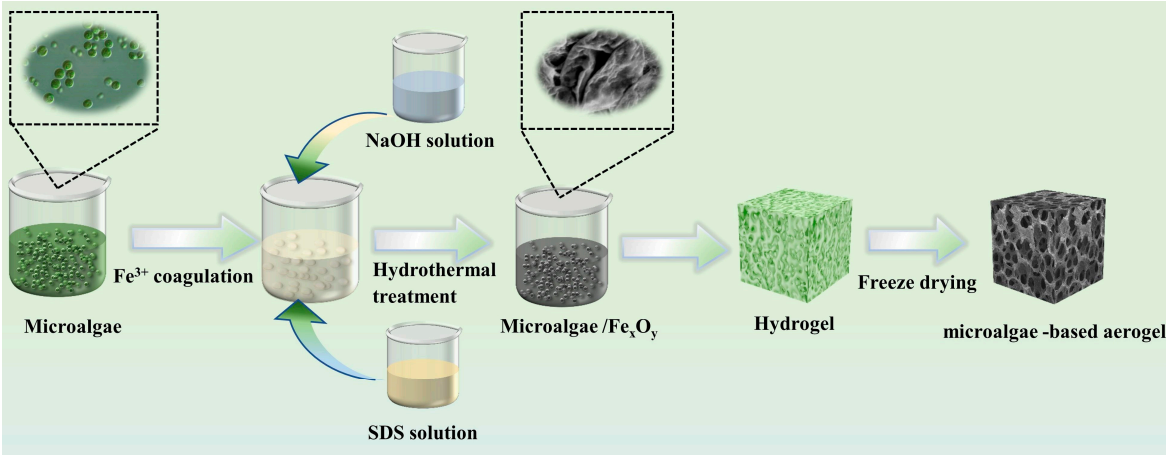


Figure 1. Schematic diagram of the preparation process of the Fe-CP aerogel.

2.3. Characterization

The morphology and composition of the aerogels were analyzed by scanning electron microscopy (SEM, S-3400 N, Tokyo, Japan) and energy dispersive X-ray spectroscopic (EDS, Oxford IE 250, London, UK) mappings, respectively. The chemical structure of the aerogel was characterized by Fourier transform infrared spectroscopy (FT-IR, Nicolet iS50, Waltham, MA, USA). The concentration of dyes was measured using a UV–vis spectrophotometer (UV-2600, Kyoto, Japan) at room temperature. The hydrophilicity of aerogel was determined by a contact angle measuring instrument (DSA25, KRUSS, Hamburg, Germany). The concentrations of Cu^{2+} were determined by ICP-OES (Optima 8300, PerkinElmer, Waltham, MA, USA).

2.4. Adsorption Experiments

Cu^{2+} was selected as a representative ion for investigating the adsorption performance of Fe-CP aerogel. In detail, the Fe-CP aerogel (50 mg) was added to Cu^{2+} solutions (50 mL, pH = 6) with different concentrations of 20, 40, 60, 100, 150, and 200 mg/L to analyze the adsorption isotherm. After shaking for 24 h at 25 °C, the concentration of Cu^{2+} in the solution was measured when it reached the adsorption equilibrium. The isotherm model and maximum adsorption quantity of Cu^{2+} adsorbed into Fe-CP aerogel were studied. Langmuir (Equation (1)) and Freundlich (Equation (2)) models were used to fit the data and further the adsorption processes.

$$c_e/q_e = 1/K_L q_{\max} + c_e/q_{\max} \quad (1)$$

$$q_e = k_F {c_e}^{1/n} \quad (2)$$

where C_e (mg/L) and q_e (mg/g) are the concentration and adsorption capacity at equilibrium. k_L (L·mg^{-1}) is the Langmuir constant, and n and k_F (mg$^{1-1/n}$·L$^{1/n}$·g^{-1}) are constants related to the intensity and capacity of the absorption process.

To investigate the adsorption kinetics, the Fe-CP aerogel (50 mg) was immersed into Cu^{2+} solution (50 mL, 100 mg/L) under stirring conditions. A certain amount of solution was taken out at different time intervals to measure the concentration of Cu^{2+}. The adsorption kinetics of Cu^{2+} onto Fe-CP aerogel were simulated with pseudo-first-order (Equation (3)), pseudo-second-order (Equation (4)), and intra-particle diffusion (Equation (5)) kinetics models, respectively.

$$q_t = q_e\left(1 - e^{-k_1 t}\right) \quad (3)$$

$$t/q_t = 1/k_2 q_e{}^2 + t/q_e \quad (4)$$

$$q_t = k_3 t^{0.5} + C \quad (5)$$

where q_e (mg/g) represents the adsorption quantity in equilibrium, k_1 (min^{-1}) and k_2 (g/(mg/min)) are the related rate constants. q_t (mg/g) is the adsorption quantity at time t. k_3 (mg/G·$h^{1/2}$) is the rate constant, and C is the intercept that is calculated from the plotting q_e vs. $t^{1/2}$.

2.5. Separation Performance of Fe-CP Aerogel for Oil/Water and Dye Solution

The oil/water and dye wastewater separation performance of the obtained Fe-CP aerogel was investigated by using a filtering apparatus. The Fe-CP aerogel was horizontally fixed in a glass funnel, and then simulated oily and dye wastewaters were poured into the glass funnel and separated by gravitational force. Ligroin, n-hexane, and kerosene (1 mL) were added into the water (99 mL) containing 10 mg Tween80 and stirred for 12 h to obtain stable oil/water emulsion. MB and RB solution with a concentration of 10 mg/L was prepared as the dye wastewater. The Fe-CP aerogel was horizontally fixed in a glass funnel, and then simulated oily and dye wastewaters were poured into the glass funnel and separated by gravitational force. During the gravity filtration test, the feed solution was added repeatedly to maintain a constant quantity and thus kept a constant flow rate. After filtration for 30 min, the flow rate was calculated. The flux (J, L/(m^2·h) was obtained using Equation (6).

$$Flux = V/S \times T \quad (6)$$

where S represents the actual area during separation, V is the volume of the permeate solution, and T is the time of separation process.

2.6. Photo-Fenton Catalytic Performance of the Fe-CP Aerogel

MB was selected as a model organic pollutant to assess the photo-Fenton catalytic capability of the Fe-CP aerogel. Specifically, the as-fabricated Fe-CP aerogel (50 mg) was added to the MB solution (50 mL, 20 mg/L) and placed in the dark condition for 90 min to achieve the adsorption equilibrium. Subsequently, after the addition of H_2O_2 (50 μL), the photo-Fenton reaction was carried out under simulated sunlight irradiation. In this process, every 10 min, the MB solution (2 mL) was collected and then the concentration measured using a UV–vis spectrophotometer.

Microorganisms widely exist in natural water bodies. Thus, the anti-biofouling property of the Fe-CP aerogel was further investigated by choosing *E. coli* as target microorganisms. *E. coli* was incubated at 37 °C in Luria-Bertani medium overnight and then diluted by fresh medium. The Fe-CP aerogel samples (2 × 2 cm^2) were immersed in the biological solution for 24 h. Then, the Fe-CP aerogel was taken out and treated with photo-Fenton, and the *E. coli* on the Fe-CP aerogel were observed by SEM.

3. Results and Discussion

3.1. Characterization of the Microalgae Aerogel

Figure 2a shows the morphology of CP cells after a hydrothermal treatment in an alkaline condition at a high temperature, which exhibit a shrink morphology with an average size of 3 μm. During this process, the protoplast inside the CP cells was removed, and hollow cell walls whose main component was cellulose were obtained. The amorphous regions of cellulose will undergo alkaline degradation through a peeling-off reaction under high pH conditions [29,30]. As shown in Figure 2b,c, many particles could be observed, which was due to the formation of Fe_xO_y inside the hollow shell. Hence, the porous shell mainly consisting of cellulose and nano-cores consisting of Fe_xO_y were formed simultaneously during the hydrothermal treatment. Then, the Fe-CP aerogel was obtained by freeze-drying. Figure 2d–f exhibit the structure of the Fe-CP aerogel as observed by SEM at different magnifications. The Fe-CP aerogel showed a porous structure with a pore size ranging from about 40 to 60 μm (Figure 2d). Moreover, the prepared Fe-CP aerogel can be

easily placed on top of the flower without destroying it, suggesting the ultra-light mass of the Fe-CP aerogel (photograph, inset of Figure 2d).

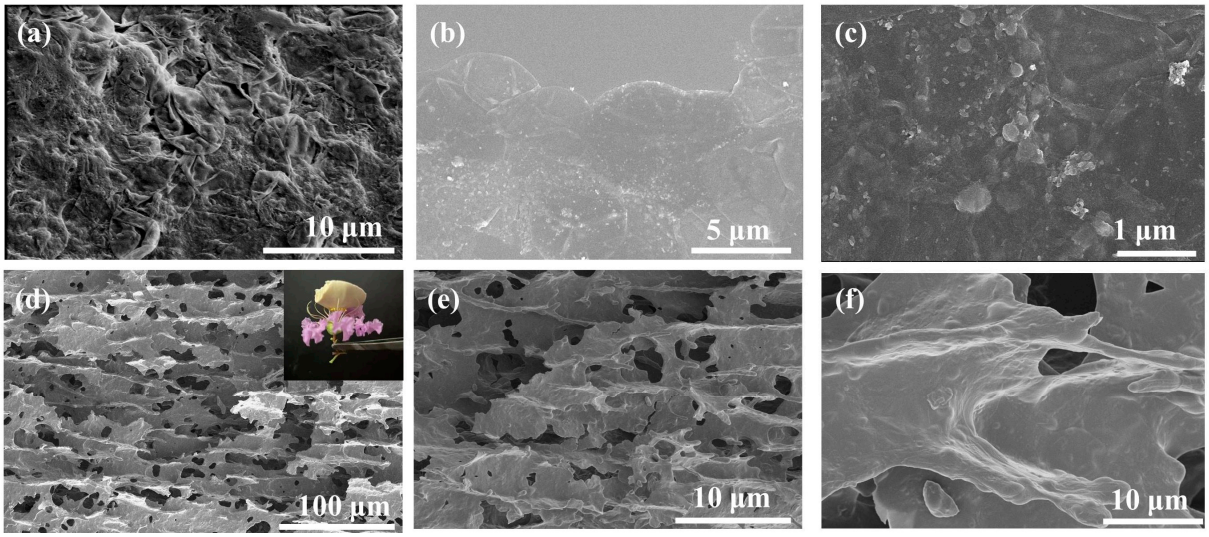


Figure 2. SEM images of the (**a**–**c**) CP cells after hydrothermal treatment under an alkaline medium and (**d**–**f**) the prepared Fe-CP aerogel.

The wettability of the Fe-CP aerogel was illustrated in Figure 3a. The water droplet was rapidly and completely adsorbed by the Fe-CP aerogel, which only took 20 microseconds, and the final water contact angle was 0°, implying that the Fe-CP aerogel possessed excellent hydrophilic properties. Figure 3b exhibits the XRD patterns of the Fe-CP aerogel. The peaks at 34.3°, 37.9°, and 40.3° corresponded to the Fe_2O_3 crystals (PDF# 76-1821), and the two peaks at 31.9° and 32.9° were due to the existence of Fe_3O_4 (PDF# 76-0958) [31].

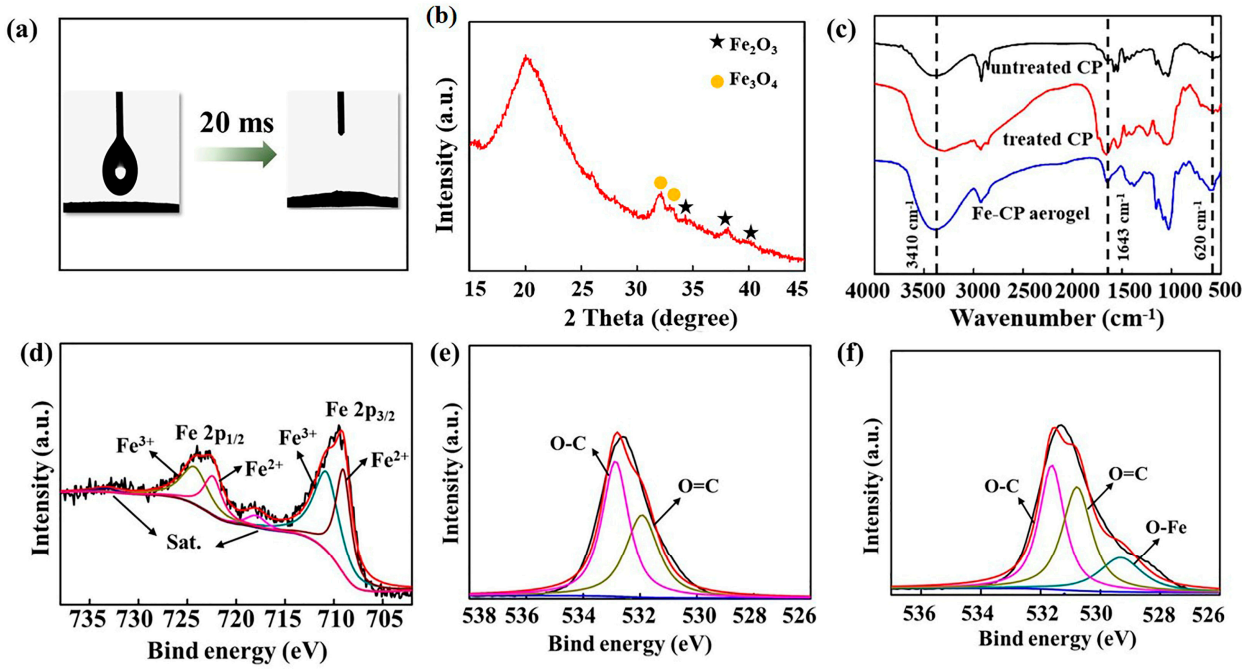


Figure 3. Characterization of the Fe-CP aerogel. (**a**) Wettability, (**b**) XRD, and (**c**) FTIR spectra of the Fe-CP aerogel. XPS patterns of (**d**) Fe 2p and (**e**) O 1s of the Fe-CP aerogel, and (**f**) O 1s of untreated CP.

The FTIR spectra of untreated CP, treated CP, and Fe-CP aerogel are exhibited in Figure 3c. The absorption peak at 3410 cm^{-1} was ascribed to the -OH groups, which became broad for the treated CP and Fe-CP aerogel. The peaks at 2924 cm^{-1} and 1384 cm^{-1} were related to the symmetric bending of the -CH or -CH_2 groups [32]. Compared with untreated CP, the peak at 1643 cm^{-1} became stronger, indicating the increased carboxylic acids after NaOH treatment. Correspondingly, the antisymmetric stretching vibration of the -CH_2 groups at 2924 cm^{-1} was weakened. Moreover, the peak at 620 cm^{-1} was attributed to the Fe-O stretching vibrations, which confirm the form of the Fe_xO_y in the treated CP and Fe-CP aerogel [33].

The chemical environment of the Fe-CP aerogel was further investigated by XPS. Figure 3d exhibits the high-resolution XPS spectra of the Fe element. The fitting characteristic peaks at 710.56 eV and 724.12 eV corresponded to the Fe^{2+}; meanwhile, the peaks at 713.45 eV and 726.25 eV were attributed to the Fe^{3+} [34,35]. In the O 1s spectrum (Figure 3e,f), the peaks at 531.9 eV and 532.8 eV were attributed to the O=C and O-C bonds, respectively. The new peak at 531.52 eV for the O-Fe bond confirmed the formation of Fe_xO_y in the Fe-CP aerogel [36].

3.2. Adsorption Performance of Microalgae Aerogel for Heavy Metal Ion

As exhibited in Figure 4a, the adsorption capacity of the Fe-CP aerogel for Cu^{2+} increased with the increased concentrations and then reached a plateau. The Freundlich and Langmuir models were used to fit the adsorption isotherm data (Figure 4c), with the higher fitting constant of the Langmuir model (0.975) than the Freundlich model (0.897) suggesting that the adsorption process belonged to monolayer adsorption (Table 1) [37]. Accordingly, the maximum adsorption capacity was calculated to be 208.3 mg/g. The adsorption kinetics were investigated through the time-dependent adsorption experiments. Figure 4b shows that the adsorption process presented a fast rate for the Fe-CP aerogel, particularly in the first 60 min, and then achieved adsorption equilibrium within 240 min. Moreover, the adsorption kinetics of Cu^{2+} on the Fe-CP aerogel could fit the pseudo-second-order model better, with an adsorption rate constant (k_2) of 0.47 × 10^{-3} g $mg^{-1}min^{-1}$ (Figure 4d), suggesting that the Cu^{2+} adsorption into the Fe-CP aerogel was a chemisorption process.

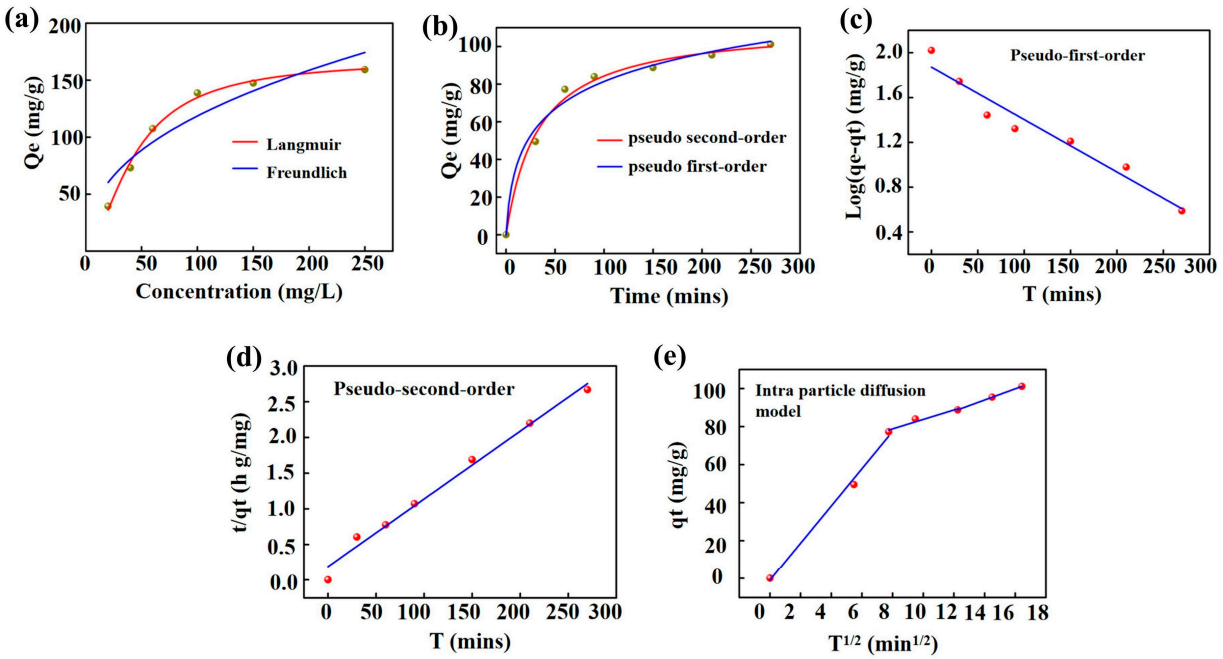


Figure 4. The influence of (**a**) concentration and (**b**) contact time on the absorption capacity of Fe-CP aerogel for Cu^{2+}. (**c**) The pseudo-first-order kinetics model, (**d**) the pseudo-second-order kinetics model, and (**e**) intra-particle diffusion plots for Cu^{2+} adsorption onto Fe-CP aerogel.

Table 1. Isotherm model parameters for adsorption of Cu^{2+} by Fe-CP aerogels.

Kinetics Models	Parameters	
Langmuir	Q_m (mg/g)	208.3
	K_L (L/mg)	0.015
	R^2	0.975
Freundlich	1/n	0.554
	K_f (L/mg)	9.124
	R^2	0.897

The diffusion mechanisms of the Cu^{2+} adsorption process were further studied through the Weber–Morris intraparticle diffusion kinetics model (Figure 4e). Three parts were observed during the adsorption process; thus, the adsorption behavior of Cu^{2+} onto the Fe-CP aerogel was affected by more than one step. The relative association constants and criterion values (R^2) of the intraparticle diffusion kinetics model were summarized in Table 2. The first part exhibited a higher slope, indicating that the Cu^{2+} diffusion to the surface of the Fe-CP aerogel was governed by the film diffusion under the driving force of the concentration difference. Moreover, the first part line avoided the origin ($c \neq 0$), implying that this process was affected by the resistance of the boundary layer [38]. The second part could be associated with the transportation of Cu^{2+} from the external surface into the inner mesopores of the Fe-CP aerogel, which was mainly controlled by the chemical reactions between Cu^{2+} and the adsorption site. In the third part, the line exhibited a small slope, which indicated that the intra-particle diffusion slowed down and reached the equilibrium stage because of the reduced Cu^{2+} concentration in the solution. In summary, the adsorption rate of Cu^{2+} onto the Fe-CP aerogel was mainly controlled by film diffusion and intra-particle diffusion.

Table 2. Parameters of kinetics models for adsorption of Cu^{2+} by Fe-CP aerogels.

Kinetics Models	Parameters		
Pseudo-first-order	Q_e (mg/g)		105.55
	K_1 (min^{-1})		0.011
	R^2		0.948
Pseudo-second-order	Q_e (mg/g)		105.26
	K_2 ($g.mg^{-1}.min^{-1}$)		0.00047
	R^2		0.987
Intra-particle diffusion	Stage 1	K_3	9.799
		C	−0.949
		R^2	0.989
	Stage 2	K_3	2.486
		C	58.902
		R^2	0.899
	Stage 3	K_3	2.951
		C	52.657
		R^2	0.999

The adsorption capacity of the Fe-CP aerogel for Cu^{2+} was compared with the aerogel-based adsorbents reported by the other literature, as summarized in Table 3. The Fe-CP aerogel exhibited superior adsorption capacity for Cu^{2+} compared to the other aerogel-based adsorbents apart from Alg-PEI. In this study, the oxygen-containing groups in the CP and Fe_xO_y can act as electron donors and transfer electrons to heavy metal ions, thus forming ionic and covalent bonds. Although some aerogel-based adsorbents exhibit higher adsorption quantity than that of the microalgae-based aerogel in our study, many of them were prepared through complex preparation processes and expensive raw materials.

Table 3. Comparison of the maximum adsorption capacity of aerogels for copper ions in related studies.

Aerogel Samples	Initial Concentration	pH	Adsorbent Dose	Q_{max} ($mg.g^{-1}$)	Ref.
PEI@wood aerogel	150 mg/L	5	1000 mg/L	59.80	[39]
ZIF-67/BC/CH	N/A	6	1000 mg/L	200.06	[40]
CS-MMT2	10 mg/L	6	1000 mg/L	86.95	[41]
Alg-PEI	0.1 mM	1–7	5000 mg/L	214.40	[42]
CGP3	100 mg/L	3–6.2	2000 mg/L	163.40	[43]
Chitosan aerogels	100 mg/L	N/A	1500 mg/L	116.70	[44]
PEI modified CCS aerogel	50 mg/L	6	400 mg/L	175.56	[45]
NFC/PEI	20 mg/L	5	300 mg/L	175.44	[46]
Fe-CP aerogel	50 mg/L	6	1000 mg/L	208.30	This work

3.3. Oil/Water Emulsion and Dye Wastewater Separation Capacity of Fe-CP Aerogel

The oil/water emulsion separation ability of the Fe-CP aerogel was investigated by separating different oil (ligroin, n-hexane, and kerosene)/water mixtures. As exhibited in Figure 5b, the Fe-CP aerogel displayed a separation efficiency higher than 99.9% for three different oil/water mixtures. Once the emulsion is in contact with the Fe-CP aerogel, water droplets can be quickly absorbed by the Fe-CP aerogel due to the preferential affinity. Thus, the water droplets are captured by the Fe-CP aerogel from the emulsions and then permeate through the Fe-CP aerogel. In this process, a stable thin water film layer that can reject oil droplets will be formed on the surface of the Fe-CP aerogel [47]. Hence, the capillary forces and gravity resulted in the water in the oil/water emulsion continuously passing through the Fe-CP aerogel. As the oil content gradually increases, oil droplets will aggregate with increased size on the surface of the Fe-CP aerogel.

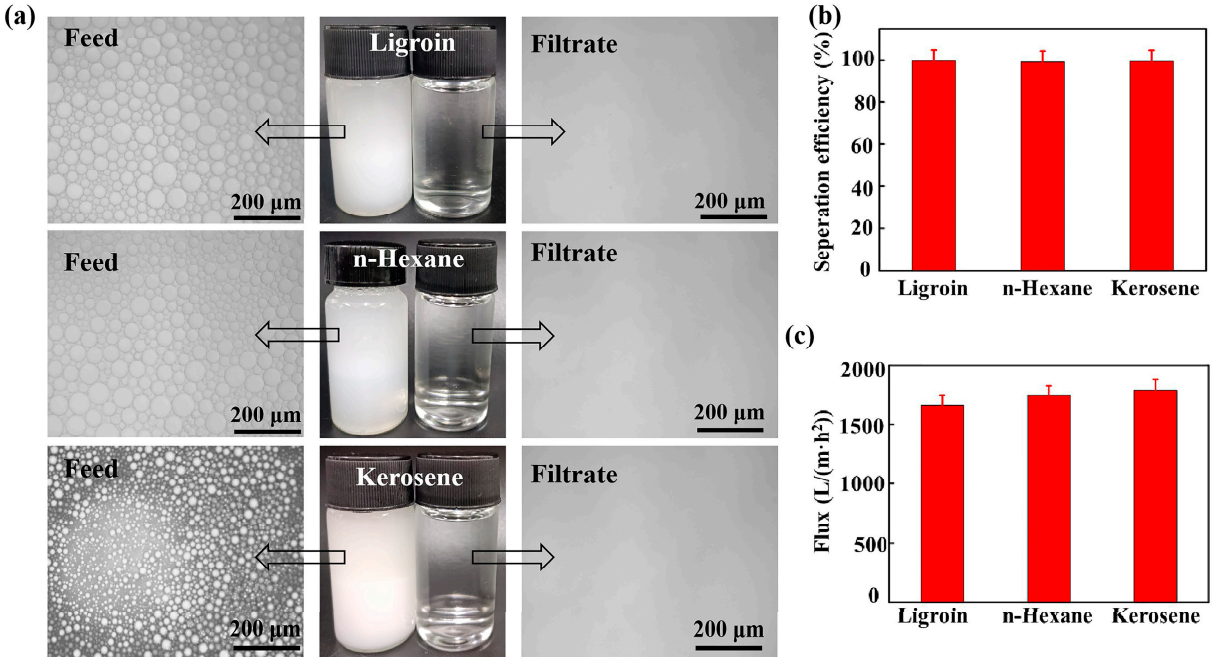


Figure 5. (**a**) The optical microscope images and the digital images of the emulsions before and after separation. (**b**) Separation efficiency and (**c**) flux of the Fe-CP aerogel for three types of oil-in-water emulsions.

There were no oil droplets observed in the transparent filtrate under the optical microscopy (Figure 5a). Moreover, the Fe-CP aerogel also possessed a high flux with a permeation flux of 1661 $L/(m^2 \cdot h)$, 1745 $L/(m^2 \cdot h)$, and 1794 $L/(m^2 \cdot h)$ for water-in-ligroin, water-in-n-hexane, and water-in-kerosene. Therefore, the excellent separation efficiency

as well as the flux of the Fe-CP aerogel for oil/water emulsion demonstrated the great potential for oil–water separation application.

Cationic dye (MB) and anionic dye (RB) solutions were prepared and used to study the removal capacity of the Fe-CP aerogel towards dyes. As shown in Figure 6a, the two different dye solutions can be almost completely decolored, with removal efficiency values of 99.1% and 95.9% for MB and RB. This result also accorded with the results of the UV–vis spectra (Figure 6c,d), which revealed remarkable selective adsorption towards the dyes. Therefore, the Fe-CP aerogel has the potential to be used for the adsorption or separation removal of dyes. The Fe-CP aerogel can adsorb dyes through hydrogen bonds and electrostatic interaction. The abundance of amino groups, carboxylate groups, and hydroxyl groups in the Fe-CP aerogel could interact with the N, O, and S atoms of the dyes, thus forming hydrogen bonding and the electrostatic interaction. The oxygen and nitrogen affinity on the Fe-CP aerogel could attract dyes through electrostatic forces. Moreover, the π system of the cellulose chain binds with the π electrons in the aromatic ring of the dye, resulting in π–π stacking interactions and electrostatic attractions.

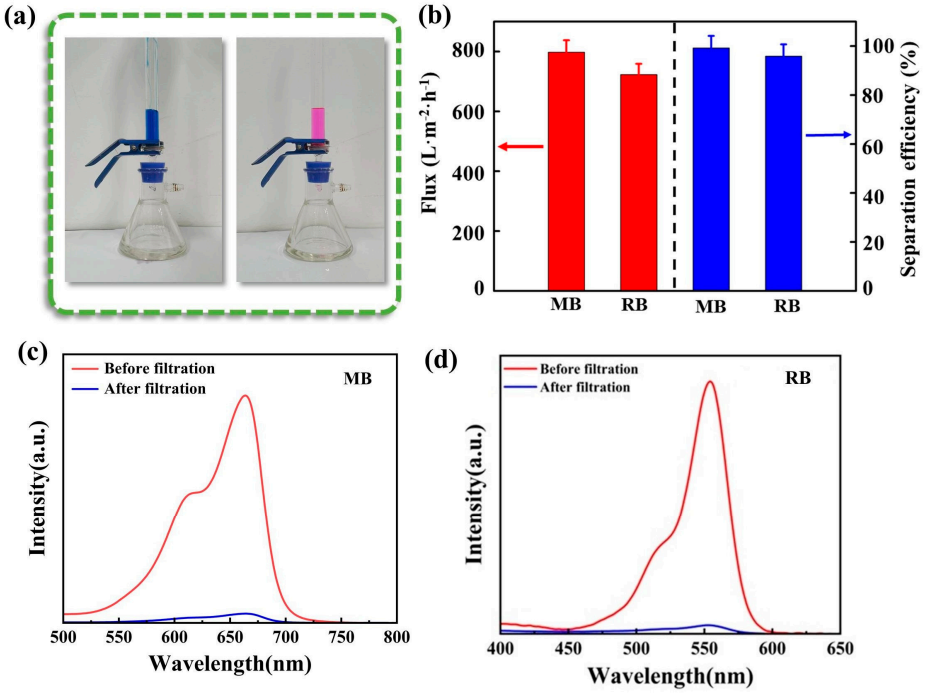


Figure 6. (**a**) The digital images of the dye waste before and after separation by Fe-CP aerogel. (**b**) Separation efficiency and flux of the Fe-CP aerogel for different dye solutions. The change in characteristic absorption peaks of (**c**) MB and (**d**) RB solutions.

3.4. Photocatalytic Capacity of Fe-CP Aerogel

The photo-Fenton catalytic ability of the Fe-CP aerogel was studied through the degradation experiment of MB. Before light irradiation, the mixture of the Fe-CP aerogel and MB solution was placed in a dark environment for 90 min with stirring to achieve the adsorption equilibrium. Figure 7a shows that the MB was degraded quickly under light irradiation. The characteristic absorption peak intensity of MB (664.8 nm) gradually decreased, and the MB almost completely degraded after irradiation for 140 min, indicating a complete MB degradation. These results indicate that the Fe-CP aerogel possessed excellent photo-Fenton degradation ability for organic dyes. Thus, the Fe-CP aerogel could be recycled by photocatalytic regeneration with high efficiency under photo-Fenton treatment.

Moreover, the antifouling ability of the Fe-CP aerogel was further evaluated by studying its antimicrobial performance. Figure 7c,d shows the microstructure of the microorganisms before and after photo-Fenton self-cleaning. Before treatment, the *E. coli* showed a

rod-shaped structure. In contrast, after the photo-Fenton treatment, most of the *E. coli* cells became flattened and decomposed/distorted, indicating the antimicrobial effects of the Fe-CP aerogel through photo-Fenton catalysis. These results indicate that the Fe-CP aerogel can effectively kill microorganisms through photo-Fenton self-cleaning. Thus, the Fe-CP aerogel possessed excellent antifouling properties and would contribute to maintaining the adsorption ability in the complex water environment.

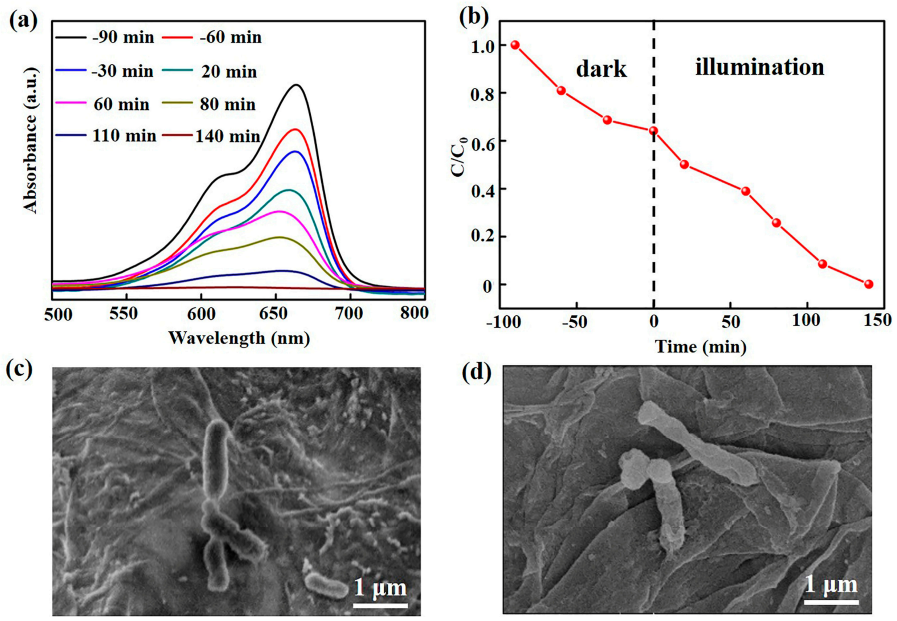


Figure 7. The photo-Fenton performance of the Fe-CP aerogel. (**a**) The changes in UV–vis spectra of MB with time during the photo-Fenton process. (**b**) The concentration changes in MB in the photo-Fenton process. The morphological changes in *E. coli* on the Fe-CP aerogel (**c**) before and (**d**) after photo-Fenton treatment.

The possible mechanisms of the photo-Fenton self-cleaning of the Fe-CP aerogel are exhibited in Figure 8. Under the visible light irradiation, the Fe_xO_y in the Fe-CP aerogel can produce electrons (^-e) and holes (h^+) [48,49]. Subsequently, the photogenerated h^+ could react with H_2O and form hydroxyl radicals (·OH). The electrons (^-e) will also react with oxygen (O_2) and produce superoxide ions (O^{2-}). The newly formed radicals with strong oxidation can degrade the contaminant and kill microorganisms and thus achieve self-cleaning.

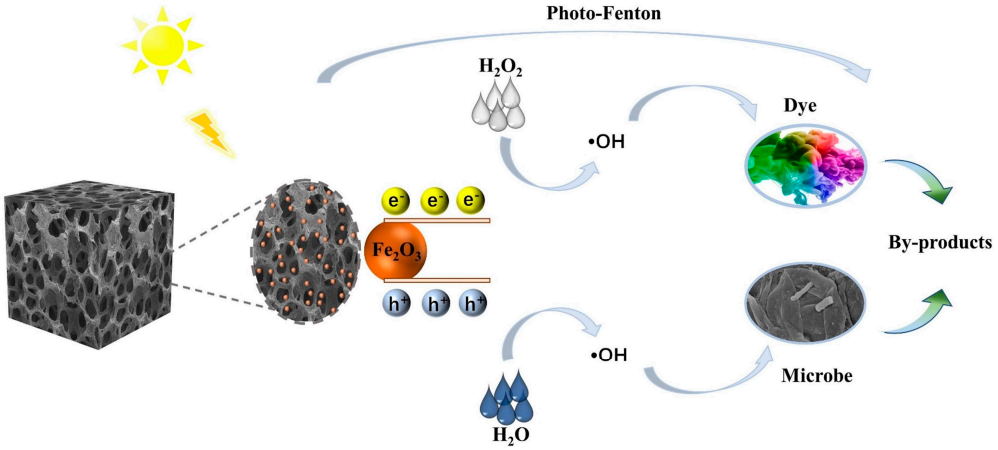


Figure 8. The mechanisms of photo-Fenton antifouling for the Fe-CP aerogel.

4. Conclusions

In summary, we prepared a novel Fe-CP aerogel as an adsorbent for the removal of pollutants from wastewater. Microspheres prepared from the iron-rich microalgae were used to prepare the Fe-CP aerogel. The Fe-CP aerogel possessed a maximum adsorption capacity of 208.3 mg/g for copper ions, and the adsorption process followed the Langmuir model. The Fe-CP aerogel also exhibited a removal efficiency of 99.1% and 95.9% for MB and RB, respectively, indicating excellent adsorption ability for dye. Due to the super-hydrophilicity, the Fe-CP aerogel can also be used for oil/water emulsions and possessed excellent separation performance. Thus, the prepared Fe-CP aerogel with rich resources, excellent adsorption capacity, and photo-Fenton self-cleaning properties demonstrated overall that it may have great potential for the practical treatment of heavy metal ions and dye wastewater.

Author Contributions: Conceptualization, X.N.; methodology, S.Z.; software, B.C.; validation, J.S. and S.Z.; formal analysis, Z.C.; investigation, B.C.; resources, J.S., B.C. and Q.W.; data curation, S.Z.; writing—original draft preparation, X.N. and J.S.; writing—review and editing, X.N. and S.Z.; visualization, J.S.; supervision, Q.W.; project administration, X.N. and Z.C.; funding acquisition, Z.C., S.Z. and Q.W. All authors have read and agreed to the published version of the manuscript.

Funding: This work was supported by the Natural Science Foundation of Fujian Province (Grant No. 2022J01942, 2023J01948); the National Innovation Demonstration Zones and Collaborative Innovation Platform Project for Fuzhou–Xiamen–Quanzhou (Grand No. 3502ZCQXT2023005); the Foreign Cooperation Projects (Industrialization) of Fujian Province (Grant No. 2023I1006, 2021I0023); University–Industry–University Cooperation Project of Fujian Province (Grant No. 2023H6036); The Young and Middle-aged Teacher Education Research Project of Fujian Province (Grant No. JAT220228); and Scientific Research Foundation of Fujian University of Technology (No. GY-Z20039, GY-Z220189).

Data Availability Statement: The data presented in this study are available on request from the corresponding author.

Conflicts of Interest: The authors declare that they have no known competing financial interests or personal relationships that may appear to influence the work reported in this paper.

References

1. Li, X.; Liu, Y.; Zhang, C.L.; Wen, T.; Zhuang, L.; Wang, X.X.; Song, G.; Chen, D.Y.; Ai, Y.J.; Hayat, T.; et al. Porous Fe_2O_3 microcubes derived from metal organic frameworks for efficient elimination of organic pollutants and heavy metal ions. *Chem. Eng. J.* **2018**, *336*, 241–252. [CrossRef]
2. Le, V.G.; Nguyen, M.N.; Nguyen, H.L.; Thai, V.A.; Le, V.R.; Manh, V.Q.; Asaithambi, P.; Woong, C.S.; Nguyen, D.D. Eco-toxicological response of algae to contaminants in aquatic environments: A review. *Environ. Chem. Lett.* **2024**, *22*, 919–939. [CrossRef]
3. Liu, X.G.; Shan, Y.Y.; Zhang, S.T.; Kong, Q.Q.; Pang, H. Application of metal organic framework in wastewater treatment. *Green Energy Environ.* **2023**, *8*, 698–721. [CrossRef]
4. Wei, Z.M.; Su, Q.; Lin, Q.Y.; Wang, X.J.; Long, S.R.; Zhang, G.; Yang, J. Multifunctional oxidized poly (arylene sulfide sulfone)/UiO-66 nanofibrous membrane with efficient adsorption/separation ability in harsh environment. *Chem. Eng. J.* **2022**, *430*, 133021. [CrossRef]
5. Fajal, S.; Dutta, S.; Ghosh, S.K. Porous organic polymers (POPs) for environmental remediation. *Mater. Horiz.* **2023**, *10*, 4083–4138. [CrossRef] [PubMed]
6. Wang, J.L.; Zhuang, S.T. Removal of cesium ions from aqueous solutions using various separation technologies. *Rev. Environ. Sci. Bio/Technol.* **2019**, *18*, 231–269. [CrossRef]
7. Vinothkumar, K.; Jyothi, M.S.; Lavanya, C.; Sakar, M.; Valiyaveettil, S.; Balakrishna, R.G. Strongly co-ordinated MOF-PSF matrix for selective adsorption, separation and photodegradation of dyes. *Chem. Eng. J.* **2022**, *428*, 132561. [CrossRef]
8. Zhang, L.P.; Liu, Z.; Zhou, X.L.; Zhang, C.; Cai, Q.W.; Xie, R.; Ju, X.J.; Wang, W.; Faraj, Y.; Chu, L.Y. Novel composite membranes for simultaneous catalytic degradation of organic contaminants and adsorption of heavy metal ions. *Sep. Purif. Technol.* **2019**, *237*, 116364. [CrossRef]
9. Chen, X.; Cui, J.; Xu, X.R.; Sun, B.J.; Zhang, L.; Dong, W.; Chen, C.T.; Sun, D.P. Bacterial cellulose/attapulgite magnetic composites as an efficient adsorbent for heavy metal ions and dye treatment. *Carbohydr. Polym.* **2020**, *229*, 115512. [CrossRef] [PubMed]
10. Elattar, R.H.; El-Deen, A.K. Porous material-based quechers: Exploring new horizons in sample preparation. *Trends Anal. Chem.* **2024**, *172*, 117571. [CrossRef]

11. Liu, Y.L.; Jin, C.; Yang, Z.Z.; Wu, G.M.; Liu, G.F.; Kong, Z.W. Recent advances in lignin-based porous materials for pollutants removal from wastewater. *Int. J. Biol. Macromol.* **2021**, *187*, 880–891. [CrossRef]
12. Lim, Y.J.; Goh, K.; Goto, A.; Zhao, Y.L.; Wang, R. Uranium and lithium extraction from seawater: Challenges and opportunities for a sustainable energy future. *J. Mater. Chem. A* **2023**, *11*, 22551–22589. [CrossRef]
13. Liu, H.W.; Li, X.Y.; Zhang, X.X.; Coulon, F.; Wang, C.Q. Harnessing the power of natural minerals: A comprehensive review of their application as heterogeneous catalysts in advanced oxidation processes for organic pollutant degradation. *Chemosphere* **2023**, *337*, 139404. [CrossRef]
14. He, W.; Cao, J.Z.; Guo, F.Y.; Guo, Z.H.; Zhou, P.G.; Wang, R.; Liang, S.; Pang, Q.Y.; Wei, B.R.; Jiao, Y.; et al. Nanostructured carboxylated-wood aerogel membrane for high-efficiency removal of Cu (II) ions from wastewater. *Chem. Eng. J.* **2023**, *468*, 143747. [CrossRef]
15. Hu, X.D.; Zhang, T.Y.; Yang, B.; Hao, M.; Chen, Z.J.; Wei, Y.; Liu, Y.B.; Wang, X.X.; Yao, J.B. Water-resistant nanocellulose/gelatin biomass aerogel for anionic/cationic dye adsorption. *Sep. Purif. Technol.* **2024**, *330*, 125367. [CrossRef]
16. Chew, K.W.; Khoo, K.S.; Foo, H.T.; Chia, S.R.; Walvekar, R.; Lim, S.S. Algae utilization and its role in the development of green cities. *Chemosphere* **2021**, *268*, 129332. [CrossRef]
17. Xu, Y.A.; Hellier, P.; Purton, S.; Baganz, F.; Ladommatos, N. Algal biomass and diesel emulsions: An alternative approach for utilizing the energy content of microalgal biomass in diesel engines. *Appl. Energy* **2016**, *172*, 80–95. [CrossRef]
18. Daneshvar, E.; Zarrinmehr, M.J.; Kousha, M.; Hashtjin, A.M.; Saratale, G.D.; Maiti, A.; Vithanage, M.; Bhatnagar, A. Hexavalent chromium removal from water by microalgal-based materials: Adsorption, desorption and recovery studies. *Bioresour. Technol.* **2019**, *293*, 122064. [CrossRef]
19. Francavilla, M.; Pineda, A.; Lin, C.S.; Franchi, M.; Trotta, P.; Romero, A.A.; Luque, R. Natural porous agar materials from macroalgae. *Carbohydr. Polym.* **2013**, *92*, 1555–1560. [CrossRef] [PubMed]
20. Shaikh, W.A.; Chakraborty, S.; Islam, R.U.; Ghfa, A.A.; Naushad, M.; Bundschuh, J.; Maity, J.P.; Mondal, N.K. Fabrication of biochar-based hybrid Ag nanocomposite from algal biomass waste for toxic dye-laden wastewater treatment. *Chemosphere* **2022**, *289*, 133243. [CrossRef]
21. Hu, X.; Liu, W.J.; Ma, L.L.; Yu, H.Q. Sustainable Conversion of Harmful Algae Biomass into a CO_2 Reduction Electrocatalyst for Two-Fold Carbon Utilization. *Environ. Sci. Technol.* **2023**, *57*, 1157–1166. [CrossRef] [PubMed]
22. Wang, S.; Lu, W.M.; Esakkimuthu, S.; Chen, H.; Yang, J.W.; Mu, M.; Gong, X. Life cycle assessment of carbon-based adsorbent preparation from algal biomass. *J. Clean. Prod.* **2023**, *427*, 139269. [CrossRef]
23. Ji, X.Y.; Luo, X.; Zhang, J.B.; Huang, D.Y. Effects of exogenous vitamin B12 on nutrient removal and protein expression of algal-bacterial consortium. *Environ. Sci. Pollut. Res.* **2021**, *28*, 15954–15965. [CrossRef] [PubMed]
24. Baskar, A.V.; Bolan, N.; Hoang, S.A.; Sooriyakumar, P.; Kumar, M.; Singh, L.; Jasemizad, T.; Padhye, L.P.; Singh, G.; Vinu, A.; et al. Recovery, regeneration and sustainable management of spent adsorbents from wastewater treatment streams: A review. *Sci. Total Environ.* **2022**, *822*, 153555. [CrossRef]
25. Zhu, S.Y.; Xu, J.; Wang, B.; Xie, J.X.; Ying, G.D.; Li, J.P.; Cheng, Z.; Li, J.; Chen, K.F. Highly efficient and rapid purification of organic dye wastewater using lignin-derived hierarchical porous carbon. *J. Colloid Interface Sci.* **2022**, *625*, 158–168. [CrossRef] [PubMed]
26. Jiang, X.Y.; Wang, H.Q.; Hu, E.; Lei, Z.W.; Fan, B.L.; Wang, Q.L. Efficient adsorption of uranium from aqueous solutions by microalgae based aerogel. *Microporous Mesoporous Mater.* **2020**, *305*, 110383. [CrossRef]
27. Tee, G.T.; Gok, X.Y.; Yong, W.F. Adsorption of pollutants in wastewater via biosorbents, nanoparticles and magnetic biosorbents: A review. *Environ. Res.* **2022**, *212*, 113248. [CrossRef] [PubMed]
28. Prasad, C.; Jeong, S.G.; Won, J.S.; Ramanjaneyulu, S.; Sangaraju, S.; Kerru, N.; Choi, H.Y. Review on recent advances in cellulose nanofibril based hybrid aerogels: Synthesis, properties and their applications. *Int. J. Biol. Macromol.* **2024**, *261*, 129460. [CrossRef]
29. Bi, L.; Luan, X.; Geng, F.L.; Xu, X.L.; Chen, Y.P.; Zhang, F. Microwave-assisted synthesis of hollow microspheres with multicomponent nanocores for heavy-metal removal and magnetic sensing. *ACS Appl. Mater. Interfaces* **2020**, *12*, 46779–46787. [CrossRef]
30. Liu, X.; Wu, Z.C.; Han, Y.H.; Han, L.J. Characteristic modification of alkalized corn stalk and contribution to the bonding mechanism of fuel briquette. *Energy* **2017**, *133*, 299–305. [CrossRef]
31. Tu, F.; Yu, Y.X.; Wang, Y.; Huang, L.Y.; Ye, D.H.; Fu, Z.Y. Preparation of SiO_2/Fe_2O_3 composite aerogels for thermal insulation enhancement. *Ceram. Int.* **2024**, *50*, 2976–2986. [CrossRef]
32. Han, X.H.; Ding, S.Q.; Zhu, L.J.; Wang, S.R. Preparation and characterization of flame-retardant and thermal insulating bio-based composite aerogels. *Energy Build.* **2023**, *278*, 112656. [CrossRef]
33. Abdullah, J.A.; Jiménez-Rosado, M.; Perez-Puyana, V.; Guerrero, A.; Romero, A. Green synthesis of Fe_xO_y nanoparticles with potential antioxidant properties. *Nanomaterials* **2022**, *12*, 2449. [CrossRef]
34. Grosvenor, A.P.; Kobe, B.A.; Biesinger, M.C.; McIntyre, N.S. Investigation of multiplet splitting of Fe 2p XPS spectra and bonding in iron compounds. *Surf. Interface Anal.* **2004**, *36*, 1564–1574. [CrossRef]
35. Ateia, E.E.; Saeid, Y.A.; Abdelmaksoud, M.K. Synthesis and characterization of $CaFe1.925Gd0.025Sm0.05O_4$/PEG core–shell nanoparticles for diverse applications. *J. Supercond. Nov. Magn.* **2023**, *36*, 1011–1024. [CrossRef]

36. Wang, T.N.; Jiao, Y.H.; He, M.C.; Peng, X.J.; Liu, P.; Ouyang, W.; Lin, C.Y.; Liu, X.T.; Xie, H.J. Efficient removal of antimony by a facile liquid-controlled strategy reinforced hematite-spinel (Fe_2O_3-$MnFe_2O_4$) composite: Construction, simulation and practical evaluation. *Chem. Eng. J.* **2023**, *451*, 138974. [CrossRef]
37. Huo, J.B.; Yu, G.C. Hexacyanoferrate-modified polyvinyl alcohol/graphene oxide aerogel as an efficient and retrievable adsorbent for cesium. *J. Mater. Sci.* **2022**, *57*, 351–365. [CrossRef]
38. Li, Q.M.; Fu, L.C.; Wang, Z.; Li, A.; Shuang, C.D.; Gao, C.Z. Synthesis and characterization of a novel magnetic cation exchange resin and its application for efficient removal of Cu^{2+} and Ni^{2+} from aqueous solutions. *J. Clean. Prod.* **2017**, *165*, 801–810. [CrossRef]
39. Meng, J.W.; Guan, H.; Dai, X.J.; Wang, X.Q. Amino-functionalized wood aerogel for efficient removal of copper ions from water. *Int. J. Polym. Sci.* **2021**, *8*, 4913226.
40. Li, D.W.; Tian, X.J.; Wang, Z.Q.; Guan, Z.; Li, X.Q.; Qiao, H.; Ke, H.Z.; Wei, Q. Multifunctional adsorbent based on metal-organic framework modified bacterial cellulose/chitosan composite aerogel for high efficient removal of heavy metal ion and organic pollutant. *Chem. Eng. J.* **2020**, *383*, 123127. [CrossRef]
41. Ye, X.; Shang, S.S.; Zhao, Y.F.; Cui, S.; Zhong, Y.; Huang, L.J. Ultra-efficient adsorption of copper ions in chitosan–montmorillonite composite aerogel at wastewater treatment. *Cellulose* **2021**, *28*, 7201–7212. [CrossRef]
42. Wang, M.; Yang, Q.; Zhao, X.Q.; Wang, Z.Q. Highly efficient removal of copper ions from water by using a novel alginate-polyethyleneimine hybrid aerogel. *Int. J. Biol. Macromol.* **2019**, *138*, 1079–1086. [CrossRef]
43. Tang, C.X.; Brodie, P.; Li, Y.Z.; Grishkewich, N.J.; Brunsting, M.; Tam, K.C. Shape recoverable and mechanically robust cellulose aerogel beads for efficient removal of copper ions. *Chem. Eng. J.* **2020**, *392*, 124821. [CrossRef]
44. Wang, Q.Z.; Li, Y. Facile and green fabrication of porous chitosan aerogels for highly efficient oil/water separation and metal ions removal from water. *J. Environ. Chem. Eng.* **2023**, *11*, 109689. [CrossRef]
45. Wang, Q.Y.; Li, L.P.; Kong, L.C.; Cai, G.Y.; Wang, P.; Zhang, J.; Zuo, W.; Tian, Y. Compressible amino-modified carboxymethyl chitosan aerogel for efficient Cu(II) adsorption from wastewater. *Sep. Purif. Technol.* **2022**, *293*, 121146. [CrossRef]
46. Li, J.; Zuo, K.; Wu, W.B.; Xu, Z.Y.; Yi, Y.G.; Jing, Y.; Dai, H.Q.; Fang, G.G. Shape memory aerogels from nanocellulose and polyethyleneimine as a novel adsorbent for removal of Cu(II) and Pb(II). *Carbohydr. Polym.* **2018**, *196*, 376–384. [CrossRef]
47. Xu, H.; Zhang, Z.; Jiang, W.; Fang, X.R.; Xia, Z.G.; Niu, H.T.; Zhou, H. Multifunctional amphibious superhydrophilic-oleophobic cellulose nanofiber aerogels for oil and water purification. *Carbohydr. Polym.* **2024**, *330*, 121774. [CrossRef]
48. He, X.H.; Wang, L.L.; Sun, S.M.; Yang, X.H.; Tian, H.Y.; Xia, Z.J.; Li, X.L.; Yan, X.L.; Pu, X.J.; Jiao, Z. Self-assembled synthesis of recyclable g-C_3N_4/NH2-MIL-53(Fe) aerogel for enhanced photocatalytic degradation of organic pollutants. *J. Alloys Compd.* **2023**, *964*, 169391. [CrossRef]
49. Mei, J.; Yuan, G.J.; Ma, Y.S.; Chen, X.; Ren, L.L. Fe-Doped alumina aerogels as a green heterogeneous catalyst for efficient degradation of organic pollutants. *Catal. Lett.* **2019**, *149*, 1874–1887. [CrossRef]

Disclaimer/Publisher's Note: The statements, opinions and data contained in all publications are solely those of the individual author(s) and contributor(s) and not of MDPI and/or the editor(s). MDPI and/or the editor(s) disclaim responsibility for any injury to people or property resulting from any ideas, methods, instructions or products referred to in the content.